

# Direct Regular-to-Chaotic Tunneling Rates Using the Fictitious Integrable System Approach

Arnd Bäcker, Roland Ketzmerick, and Steffen Löck

Institut für Theoretische Physik, Technische Universität Dresden, 01062 Dresden, Germany

August 13, 2018

## Abstract

In systems with a mixed phase space, where regular and chaotic motion coexists, regular states are coupled to the chaotic region by dynamical tunneling. We give an overview on the determination of direct regular-to-chaotic tunneling rates using the fictitious integrable system approach. This approach is applied to different kicked systems, including the standard map, and successfully compared with numerical data.

*This text corresponds to Chapter 6 of the book: Dynamical Tunneling - Theory and Experiment, edited by S. Keshavamurthy and P. Schlagheck [Taylor and Francis CRC (2011)] [1]. For a more extensive exposition see [Phys. Rev. E 82, 056208 (2010); arXiv:1009.0418v2].*

## 1 Introduction

Tunneling is one of the most fundamental manifestations of quantum mechanics. For 1D systems the theoretical description is well established by the Wentzel-Kramers-Brillouin (WKB) method and related approaches [2, 3]. However, for higher dimensional systems no such simple description exists. In these systems typically regular and chaotic motion coexists and in the two-dimensional case regular tori are absolute barriers to the motion. Quantum mechanically, the eigenfunctions either concentrate within the regular islands or in the chaotic sea, as expected from the semiclassical eigenfunction hypothesis [4, 5, 6]. These eigenfunctions are coupled by so-called dynamical tunneling [7] through the dynamically generated barriers in phase space. In particular, this leads to a substantial enhancement of tunneling rates between phase-space regions of regular motion due to the presence of chaotic motion, which was termed chaos-assisted tunneling [8, 9, 10]. Such dynamical tunneling processes are ubiquitous in molecular physics and were realized with microwave cavities [11] and cold atoms in periodically modulated optical lattices [12, 13].

In the quantum regime,  $h_{\text{eff}} \lesssim A$ , where the effective Planck constant  $h_{\text{eff}}$  is smaller but still comparable to the area of the regular island  $A$ , the process of tunneling into the chaotic region is dominated by a *direct regular-to-chaotic tunneling* mechanism [14, 15, 16, 17]. For the prediction of tunneling rates the fictitious integrable system approach was introduced recently [17]. It relies on a fictitious integrable system [9, 15] that resembles the

regular dynamics within the island under consideration. The approach has been applied to quantum maps [17], billiard systems [18], and the annular microcavity [19]. In the semiclassical regime,  $\hbar_{\text{eff}} \ll A$ , however, the direct tunneling contribution alone is typically not sufficient to describe the observed tunneling rates, because nonlinear resonance chains within the regular island lead to resonance-assisted tunneling [20, 21, 22, 23]. Recently, a combined prediction of dynamical tunneling rates from regular to chaotic phase-space regions was derived [24], which combines the direct regular-to-chaotic tunneling mechanism in the quantum regime with an improved resonance-assisted tunneling theory in the semiclassical regime. In this text we concentrate on the fictitious integrable system approach for the theoretical description of the direct regular-to-chaotic tunneling mechanism and how it can be applied analytically, semiclassically, and numerically to quantum maps.

This text is organized as follows: We start by defining different convenient kicked systems, their quantization, and the numerical determination of tunneling rates. In Sec. 3 we describe the approach to determine dynamical tunneling rates by using a fictitious integrable system. In Sec. 4 we apply this theory to the previously introduced systems and compare its results with numerical data. We conclude with a brief summary.

## 2 Kicked systems

Kicked systems are particularly suited to study classical and quantum effects appearing in a mixed phase space as they can be easily treated analytically and numerically. In contrast to time-independent systems, where at least two degrees of freedom are necessary to break integrability, one-dimensional driven systems can show chaotic motion. We consider time-periodic one-dimensional kicked systems

$$H(q, p, t) = T(p) + V(q) \sum_{n \in \mathbb{Z}} \tau \delta(t - n\tau), \quad (1)$$

which are described by the kinetic energy  $T(p)$  and the potential  $V(q)$  which is applied once per kick period  $\tau = 1$ . The classical dynamics of a kicked system is given by its stroboscopic mapping, e.g., evaluated just after each kick

$$\begin{aligned} q_{n+1} &= q_n + T'(p_n), \\ p_{n+1} &= p_n - V'(q_{n+1}). \end{aligned} \quad (2)$$

It maps the phase-space coordinates after the  $n$ th kick to those after the  $(n + 1)$ th kick. For the stroboscopic mapping we consider a compact phase space with periodic boundary conditions for  $q \in [-1/2, 1/2]$  and  $p \in [-1/2, 1/2]$ . The phase space generally consists of regions with regular motion surrounded by chaotic dynamics, see Fig. 1(b). We focus on the situation of just one regular island embedded in the chaotic sea, Fig. 2(a),(b). At the center of the island one has an elliptic fixed point, which is surrounded by invariant regular tori. Classically, a particle within a regular island will never enter into the chaotic region and vice versa, i.e. tori form absolute barriers to the motion.

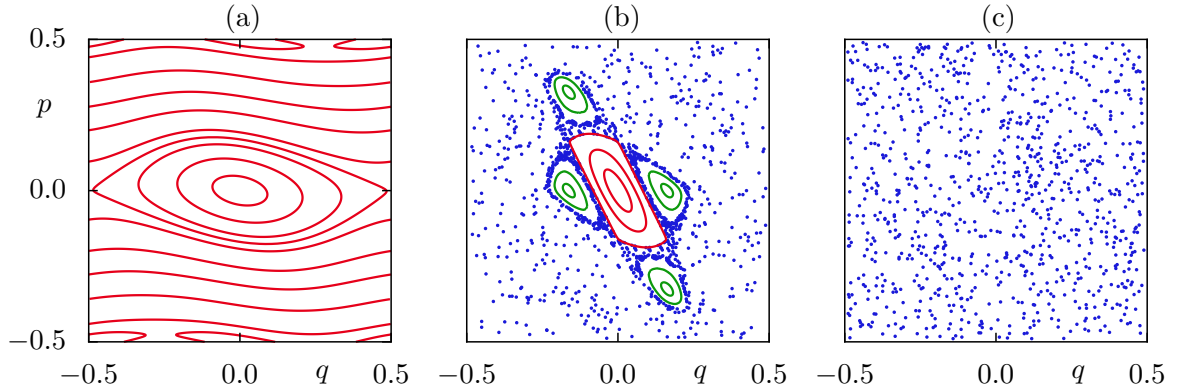


Figure 1: Phase space of the standard map for (a)  $\kappa = 0.3$ , (b)  $\kappa = 2.4$ , and (c)  $\kappa = 8$ . In (a) the system is nearly integrable. Most of the phase space is filled by invariant tori (lines). The second figure (b) shows a mixed phase space with regular motion (lines) and chaotic motion (dots). The four small islands surrounding the central island form a nonlinear resonance chain. In the chaotic sea partial barriers exist, which is reflected by the different densities of chaotic points. For large values of  $\kappa$  as in (c) the phase space seems macroscopically chaotic.

## 2.1 Standard map

The paradigmatic model of an area preserving map is the standard map, defined by Eq. (2) with the functions

$$T'(p) = p, \quad (3)$$

$$V'(q) = \frac{\kappa}{2\pi} \sin(2\pi q). \quad (4)$$

For  $\kappa = 0$  the system is integrable and the dynamics takes place on invariant tori with constant momentum. For small  $\kappa > 0$ , see Fig. 1(a), the system is no longer integrable. However, as stated by the Kolmogorov-Arnold-Moser (KAM) theorem [25], many invariant tori persist. In between these tori sequences of stable and unstable fixed points emerge, which is described by the Poincaré-Birkhoff theorem [26]. The stable fixed points of such a sequence form so-called nonlinear resonance chains, see Fig. 1(b), while in the vicinity of the unstable fixed points typically chaotic dynamics is observed. For larger  $\kappa$  more and more regular tori break up and the chaotic dynamics occupies a larger area of phase space. At  $\kappa \approx 3$  one large regular region (“regular island”) is surrounded by a region of chaotic dynamics (“chaotic sea”). At the border of the regular island a hierarchical region exists, where self-similar structures of regular and chaotic dynamics are found on all scales. Also in the chaotic sea additional structures can be found. Here, partial barriers limit the classical flux between different regions of chaotic motion caused by the stable and unstable manifolds of unstable periodic orbits or caused by cantori, which are the remnants of regular tori [27]. For even larger  $\kappa$  the regular islands disappear and the motion seems macroscopically chaotic, see Fig. 1(c).

All these structures in phase space, such as nonlinear resonances, the hierarchical regular-to-chaotic transition region, and partial barriers within the chaotic sea, have an

influence on the dynamical tunneling process from the regular island to the chaotic sea. In order to quantitatively understand dynamical tunneling in systems with a mixed phase space, it is helpful to first consider simpler model systems. By designing maps such that the phase-space structures can be switched on and off one-by-one it is possible to study their influence on the dynamical tunneling process separately. Afterwards the results can be tested using the generic example of the standard map.

## 2.2 Designed maps

Our aim is to introduce kicked systems which are designed such that their phase space is particularly simple. It shows one regular island embedded in the chaotic sea, with very small nonlinear resonance chains within the regular island, a narrow hierarchical region, and without relevant partial barriers in the chaotic component. For such a system it is possible to study the direct regular-to-chaotic tunneling process without additional effects caused by these structures as long as  $h_{\text{eff}}$  is big enough. To this end we define the family of maps  $\mathcal{D}$ , according to Eq. (2), with an appropriate choice of the functions  $T'(p)$  and  $V'(q)$  [28, 29, 17, 24]. For this we first introduce

$$t'(p) = \frac{1}{2} \pm (1 - 2p) \quad \text{for} \quad 0 < \pm p < \frac{1}{2}, \quad (5)$$

$$v'(q) = -rq + Rq^2 \quad \text{for} \quad -\frac{1}{2} < q < \frac{1}{2} \quad (6)$$

with  $0 < r < 2$  and  $R \geq 0$ . Considering periodic boundary conditions the functions  $t'(p)$  and  $v'(q)$  show discontinuities at  $p = 0, \pm 1/2$  and  $q = \pm 1/2$ , respectively. In order to avoid these discontinuities we smooth the periodically extended functions  $v'(q)$  and  $t'(q)$  with a Gaussian,

$$G(z) = \frac{1}{\sqrt{2\pi\varepsilon^2}} \exp\left(-\frac{z^2}{2\varepsilon^2}\right), \quad (7)$$

resulting in analytic functions

$$T'(p) = \int dz t'(z)G(p - z), \quad (8)$$

$$V'(q) = \int dz v'(z)G(q - z), \quad (9)$$

which are periodic with respect to the phase-space unit cell. With this we obtain the maps  $\mathcal{D}$  depending on the parameters  $r$ ,  $R$ , and the smoothing strength  $\varepsilon$ . The smoothing  $\varepsilon$  determines the size of the hierarchical region at the border of the regular island. Tuning the parameters  $r$  and  $R$  one can find situations, where all nonlinear resonance chains inside the regular island are small.

For  $R = 0$  both functions  $v'(q)$  and  $t'(p)$  are linear in  $q$  and  $p$ , respectively. In this case we find a harmonic oscillator-like regular island with elliptic invariant tori and constant rotation number. We choose the parameters  $r = 0.46$ ,  $R = 0$ , and  $\varepsilon = 0.005$  for which the phase space of the resulting map  $\mathcal{D}_{\text{ho}}$  is shown in Fig. 2(a).

In typical systems the rotation number of regular tori changes from the center of the regular region to its border which typically has a non-elliptic shape. Such a situation can

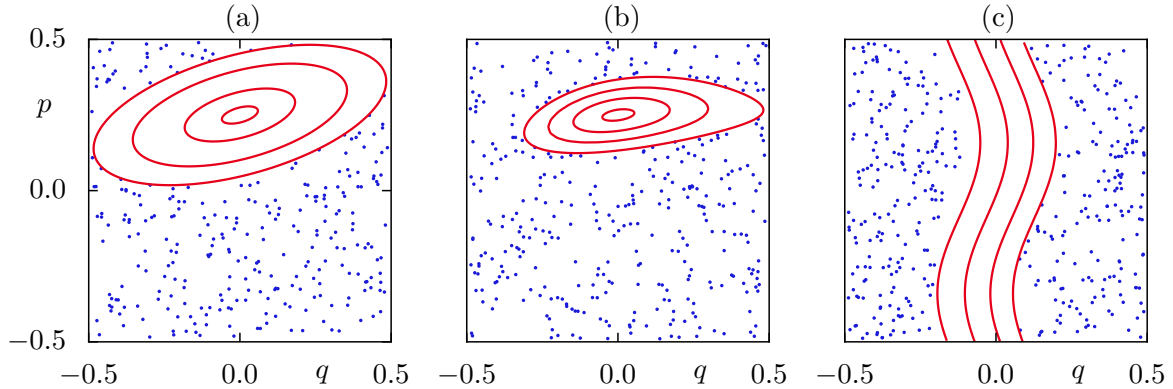


Figure 2: Phase space of (a) the designed map  $\mathcal{D}_{\text{ho}}$  with a harmonic oscillator-like regular island, (b)  $\mathcal{D}_{\text{d}}$  with a deformed regular island, and (c)  $\mathcal{D}_{\text{rs}}$  with a regular stripe. For parameters see text.

be achieved for the family of maps  $\mathcal{D}$  with the parameter  $R \neq 0$ . For most combinations of the parameters  $r$  and  $R$  resonance structures appear inside the regular island. They limit the  $h_{\text{eff}}$ -regime in which the direct regular-to-chaotic tunneling process dominates. Hence, we choose a situation in which the nonlinear resonances are small such that their influence on the tunneling process is expected only at small  $h_{\text{eff}}$ . The phase space of the map  $\mathcal{D}_{\text{d}}$ , obtained for  $r = 0.26$ ,  $R = 0.4$ , and  $\varepsilon = 0.005$ , is shown in Fig. 2(b).

Another designed kicked system was introduced in Refs. [30, 31, 32]. Here the regular region consists of a stripe in phase space, see Fig. 2(c). In our notation the mapping, Eq. (2), is specified by the functions

$$V'(q) = -\frac{1}{2\pi} \left( 8\pi a q + d_1 - d_2 + \frac{1}{2} [8\pi a q - \omega + d_1] \tanh[b(8\pi q - q_d)] + \frac{1}{2} [-8\pi a q + \omega + d_2] \tanh[b(8\pi q + q_d)] \right) \quad (10)$$

$$T'(p) = -\frac{\kappa}{8\pi} \sin(2\pi p). \quad (11)$$

The kinetic energy  $T(p)$  is periodic with respect to the phase space unit cell. We label the resulting map with a regular stripe by  $\mathcal{D}_{\text{rs}}$  using the parameters  $a = 5$ ,  $b = 100$ ,  $d_1 = -24$ ,  $d_2 = -26$ ,  $\omega = 1$ ,  $q_d = 5$ , and  $\kappa = 3$ .

The map  $\mathcal{D}_{\text{rs}}$  is similar to the system  $\mathcal{D}_{\text{ho}}$  as it also destroys the integrable region by smoothly changing the function  $V'(q)$ , here at  $|q| = q_d/(8\pi)$ . For  $|q| < q_d/(8\pi)$  the potential term is almost linear while it tends to the standard map for  $|q| > q_d/(8\pi)$ . The parameter  $b$  determines the width of the transition region.

## 2.3 Quantization

Quantum mechanically kicked systems are described by the unitary time-evolution operator  $U$  [33]. It can be written as  $U = U_V U_T$  with

$$U_V = e^{-iV(q)/\hbar_{\text{eff}}}, \quad (12)$$

$$U_T = e^{-iT(p)/\hbar_{\text{eff}}}. \quad (13)$$

Its eigenstates  $|\psi_n\rangle$  and quasi-energies  $\varphi_n$  are determined by

$$U|\psi_n\rangle = e^{i\varphi_n}|\psi_n\rangle. \quad (14)$$

We consider a compact phase space with periodic boundary conditions in  $q$  and  $p$ . This implies that the effective Planck constant can take only the discrete values [34]

$$h_{\text{eff}} = \frac{1}{N}, \quad (15)$$

where  $N$  is the dimension of the Hilbert space. In addition the position and momentum coordinates are quantized according to

$$q_k = \frac{k}{N} - \frac{1}{2}, \quad (16)$$

$$p_l = \frac{l}{N} - \frac{1}{2} \quad (17)$$

with  $k, l = 0, \dots, N - 1$ .

For systems with a mixed phase space, in the semiclassical limit ( $h_{\text{eff}} \rightarrow 0$ ), the semiclassical eigenfunction hypothesis [4, 5, 6] implies that the eigenstates  $|\psi_n\rangle$  can be classified as either regular or chaotic according to the phase-space region on which they concentrate, see Fig. 3. In order to understand the behavior of eigenstates away from the semiclassical limit, i.e. at finite values of the effective Planck constant  $h_{\text{eff}}$ , one has to compare the size of phase-space structures with  $h_{\text{eff}}$ .

The so-called regular states are concentrated on tori within the regular island and fulfill the Bohr-Sommerfeld type quantization condition

$$\oint p dq = h_{\text{eff}} \left( m + \frac{1}{2} \right), \quad m = 0, \dots, N_{\text{reg}} - 1. \quad (18)$$

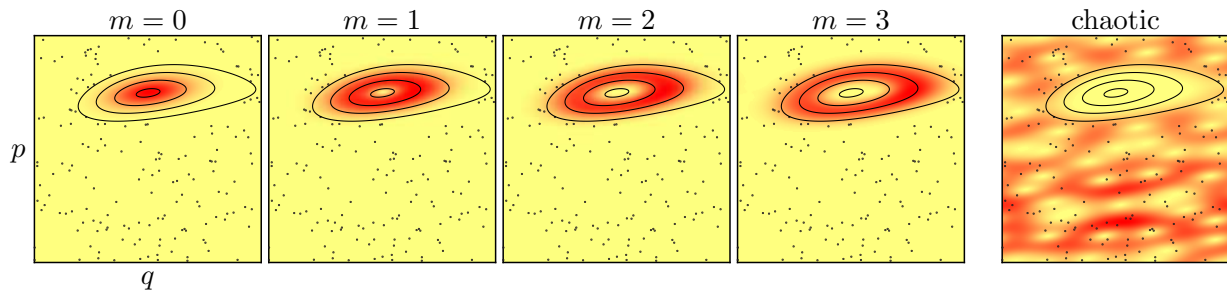


Figure 3: Husimi representation of eigenfunctions of the map  $\mathcal{D}_d$  for  $h_{\text{eff}} = 1/50$ . The regular ground state  $m = 0$  and the first three excited states  $m = 1, 2, 3$  as well as a chaotic state are shown.

For a given value of  $h_{\text{eff}}$  there exist  $N_{\text{reg}}$  of such regular states, where  $N_{\text{reg}} = \lfloor A/h_{\text{eff}} + 1/2 \rfloor$  and  $A$  is the area of the regular island. The  $N_{\text{ch}} = N - N_{\text{reg}}$  chaotic states extend over the chaotic sea. Due to dynamical tunneling, however, the regular and chaotic eigenfunctions of  $U$  always have a small component in the other region of phase space, respectively. This is most clearly seen for hybrid states which even have the same weight in each of the components as they are involved in an avoided level crossing.

## 2.4 Numerical determination of tunneling rates

The structure of the considered phase space, with one regular island surrounded by the chaotic sea, allows for the determination of tunneling rates by introducing absorption somewhere in the chaotic region of phase space. For quantum maps, this can for example be realized by using a non-unitary open quantum map [35]

$$U^o = PUP, \quad (19)$$

where  $P$  is a projection operator onto the complement of the absorbing region.

While the eigenvalues of  $U$  are located on the unit circle the eigenvalues of  $U^o$  are inside the unit circle as  $U^o$  is sub-unitary. The eigenequation of  $U^o$  reads

$$U^o |\psi_n^s\rangle = z_n |\psi_n^s\rangle \quad (20)$$

with eigenvalues

$$z_n = e^{i(\varphi_n + i\frac{\gamma_n}{2})}. \quad (21)$$

The decay rates are characterized by the imaginary part of the quasi-energies in Eq. (21) and one has

$$\gamma_m = -2 \log |z_m| \approx 2(1 - |z_m|). \quad (22)$$

If the chaotic region does not contain partial barriers and shows no dynamical localization, it is justified to assume that the rate of escaping the regular island is equal to the rate of leaving through the absorbing regions located in the chaotic sea. Then, the location of the absorbing regions in the chaotic part of phase space has no effect on the tunneling rates.

In generic systems, however, partial barriers will appear in the chaotic region of phase space. The additional transition through these structures further limits the quantum transport such that the calculated decay through the absorbing region occurs slower than the decay from the regular island to the neighboring chaotic sea. Similarly dynamical localization in the chaotic region may slow down the decay. The influence of partial barriers and dynamical localization on the tunneling process is an open problem. Here we will suppress their influence, if necessary, by moving the absorbing regions closer to the regular island.

In Fig. 4 tunneling rates are determined numerically by opening the system for the map  $\mathcal{D}_{\text{ho}}$  (dots). These agree very well with an analytical prediction (lines), Eq. (27), which is derived in the next section.

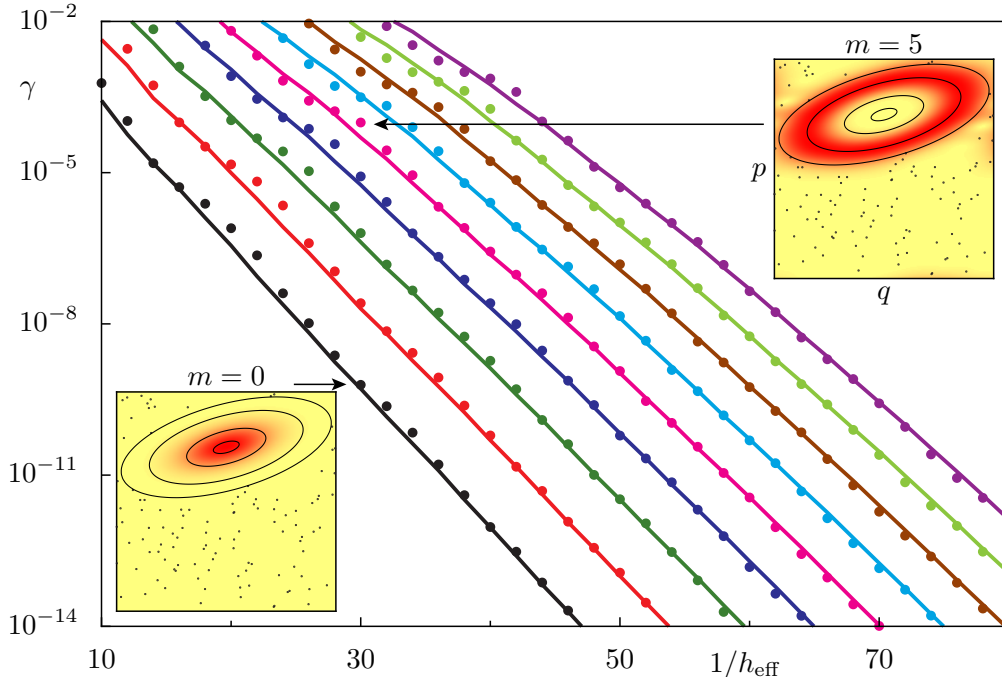


Figure 4: Numerical data (dots) for  $m \leq 8$  for the map  $\mathcal{D}_{\text{ho}}$  with a harmonic oscillator-like island. Comparison with Eq. (27) (lines), see Sec. 3.1 for its derivation. The insets show Husimi functions of the regular states for the quantum numbers  $m = 0$  and  $m = 5$  at  $1/h_{\text{eff}} = 30$ .

### 3 Tunneling using a fictitious integrable system

Dynamical tunneling in systems with a mixed phase space couples the regular island and the chaotic sea, which are classically separated. This coupling can be quantified by tunneling rates  $\gamma_m$  which describe the decay of regular states to the chaotic sea. To define these tunneling rates one can consider a wave packet started on the  $m$ th quantized torus in the regular island coupled to a continuum of chaotic states, as in the case for an infinite chaotic sea or in the presence of an absorbing region somewhere in the chaotic sea. Its decay  $e^{-\gamma_m t}$  is described by a tunneling rate  $\gamma_m$ . For systems with a finite phase space this exponential decay occurs at most up to the Heisenberg time  $\tau_H = h_{\text{eff}}/\Delta_{\text{ch}}$ , where  $\Delta_{\text{ch}}$  is the mean level spacing of the chaotic states.

In the quantum regime,  $h_{\text{eff}} \lesssim A$ , where  $h_{\text{eff}}$  is smaller but comparable to the area  $A$  of the regular island, the rates  $\gamma_m$  are dominated by the direct regular-to-chaotic tunneling mechanism, while contributions from resonance-assisted tunneling are negligible. We concentrate on situations where additional phase-space structures within the chaotic sea are not relevant for tunneling. In the following we derive a prediction for the direct regular-to-chaotic tunneling rates using the fictitious integrable system approach [17].

### 3.1 Derivation

In order to find a prediction for the direct regular-to-chaotic tunneling rates we decompose the Hilbert space of the quantum map  $U$  into two parts which correspond to the regular and chaotic regions. While classically such a decomposition is unique (neglecting tiny phase-space structures), quantum mechanically this is not the case due to the uncertainty principle. We find a decomposition by introducing a fictitious integrable system  $U_{\text{reg}}$  (a related idea was presented in Refs. [9, 15, 16]). It has to be chosen such that its dynamics resembles the classical motion corresponding to  $U$  within the regular island as closely as possible and continues this regular dynamics beyond the regular island of  $U$ , see Fig. 5(a),(d). The eigenstates  $|\psi_{\text{reg}}^m\rangle$  of  $U_{\text{reg}}$  are purely regular in the sense that they are localized on the  $m$ th quantized torus of the regular region and continue to decay beyond this regular region, see Fig. 5(e). This is the decisive property of  $|\psi_{\text{reg}}^m\rangle$  which have no chaotic admixture, in contrast to the predominantly regular eigenstates of  $U$ , see Fig. 5(b). The explicit construction of  $U_{\text{reg}}$  is discussed in Sec. 3.2.

With the eigenstates  $|\psi_{\text{reg}}^m\rangle$  of  $U_{\text{reg}}$ ,  $U_{\text{reg}}|\psi_{\text{reg}}^m\rangle = e^{i\varphi_{\text{reg}}^m}|\psi_{\text{reg}}^m\rangle$ , we define a projection operator

$$P_{\text{reg}} := \sum_{m=0}^{N_{\text{reg}}-1} |\psi_{\text{reg}}^m\rangle\langle\psi_{\text{reg}}^m|, \quad (23)$$

using the first  $N_{\text{reg}}$  regular states of  $U_{\text{reg}}$  which approximately projects onto the regular island corresponding to  $U$ . The orthogonal projector

$$P_{\text{ch}} := \mathbb{1} - P_{\text{reg}} \quad (24)$$

approximately projects onto the chaotic phase-space region. These projectors,  $P_{\text{reg}}$  and  $P_{\text{ch}}$ , define our decomposition of the Hilbert space into a regular and a chaotic subspace.

Introducing an orthonormal basis  $|\psi_{\text{ch}}\rangle$  in the chaotic subspace we can write  $P_{\text{ch}} = \sum_{\text{ch}} |\psi_{\text{ch}}\rangle\langle\psi_{\text{ch}}|$ . Here we sum over all  $N_{\text{ch}} = N - N_{\text{reg}}$  states  $|\psi_{\text{ch}}\rangle$ , see Fig. 5(f) for an example. Hence, the coupling matrix element  $v_{\text{ch},m}$  between a purely regular state  $|\psi_{\text{reg}}^m\rangle$  and any chaotic basis state  $|\psi_{\text{ch}}\rangle$  is

$$v_{\text{ch},m} = \langle\psi_{\text{ch}}|U|\psi_{\text{reg}}^m\rangle. \quad (25)$$

The tunneling rate is obtained using a dimensionless version of Fermi's golden rule,

$$\gamma_m = \sum_{\text{ch}} |v_{\text{ch},m}|^2, \quad (26)$$

where the sum is over all chaotic basis states  $|\psi_{\text{ch}}\rangle$  and thus averages the modulus squared of the fluctuating matrix elements  $v_{\text{ch},m}$ . Here we apply Fermi's golden rule in the case of a discrete spectrum, which is possible if one considers the decay  $e^{-\gamma_m t}$  up to the Heisenberg time  $\tau_H = \hbar_{\text{eff}}/\Delta_{\text{ch}}$  only. Inserting Eq. (25) we obtain

$$\gamma_m = \|P_{\text{ch}}U|\psi_{\text{reg}}^m\rangle\|^2 = \|(\mathbb{1} - P_{\text{reg}})U|\psi_{\text{reg}}^m\rangle\|^2 \quad (27)$$

as the basis of all our following investigations. It allows for the prediction of tunneling rates from a regular state localized on the  $m$ th quantized torus to the chaotic sea. Equation (27) confirms the intuition that the tunneling rates are determined by the amount of probability

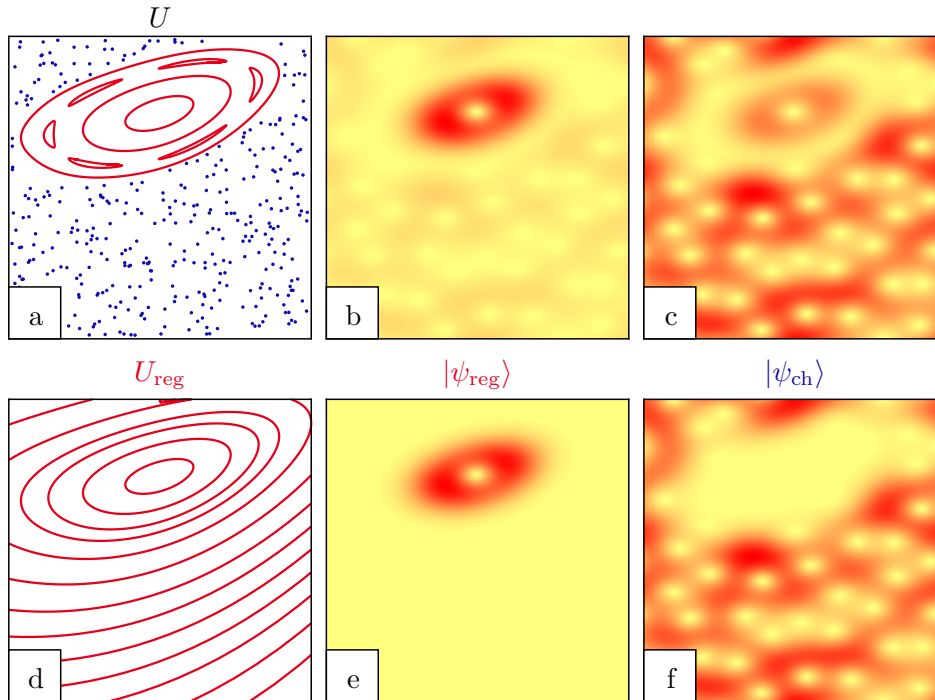


Figure 5: (a) Illustration of the classical phase space corresponding to some mixed quantum map  $U$  together with the Husimi representation of (b) a regular and (c) a chaotic eigenstate of  $U$  which both have a small component in the other region. (d) Illustration of the classical phase space of the fictitious integrable system  $U_{\text{reg}}$ . (e) Eigenstates  $|\psi_{\text{reg}}\rangle$  of  $U_{\text{reg}}$  are purely regular while (f) the basis states  $|\psi_{\text{ch}}\rangle$  are localized in the chaotic region of phase space.

of  $|\psi_{\text{reg}}^m\rangle$  that is transferred to the chaotic region after one application of the time evolution operator  $U$ . In Eq. (27) properties of the fictitious integrable system  $U_{\text{reg}}$  and the chaotic projector  $P_{\text{ch}} = \mathbb{1} - P_{\text{reg}}$  enter, which rely on the chosen decomposition of Hilbert space.

In cases where one finds a fictitious integrable system  $U_{\text{reg}}$  which resembles the dynamics within the regular island of  $U$  with very high accuracy, Eq. (27) can be approximated as

$$\gamma_m \approx \|(U - U_{\text{reg}})|\psi_{\text{reg}}^m\rangle\|^2, \quad (28)$$

using  $P_{\text{reg}}U|\psi_{\text{reg}}^m\rangle \approx P_{\text{reg}}U_{\text{reg}}|\psi_{\text{reg}}^m\rangle = U_{\text{reg}}|\psi_{\text{reg}}^m\rangle$ . Instead of the operator product  $P_{\text{ch}}U$  in Eq. (27) the difference  $U - U_{\text{reg}}$  enters in Eq. (28). It allows for further derivations, which are presented in Sec. 3.3.

### 3.2 Fictitious integrable system

The most difficult step in the application of Eq. (27) to a given system is the determination of the fictitious integrable system  $U_{\text{reg}}$ . On the one hand its dynamics should resemble the classical motion of the considered mixed system within the regular island as closely as possible. As a result the contour lines of the corresponding integrable Hamiltonian

$H_{\text{reg}}$ , Fig. 5(d), approximate the KAM-curves of the classically mixed system, Fig. 5(a), in phase space. This resemblance is not possible with arbitrary precision as the integrable approximation does not contain, e.g., nonlinear resonance chains and small embedded chaotic regions. Moreover, it cannot account for the hierarchical regular-to-chaotic transition region at the border of the regular island. Similar problems appear for the analytic continuation of a regular torus into complex space due to the existence of natural boundaries [36, 37, 30, 31, 38, 20, 21, 22]. However, for not too small  $h_{\text{eff}}$ , where these small structures are not yet resolved, an integrable approximation with finite accuracy turns out to be sufficient for a prediction of the tunneling rates.

On the other hand the integrable dynamics of  $H_{\text{reg}}$  should extrapolate smoothly beyond the regular island of  $H$ . This is essential for the quantum eigenstates of  $H_{\text{reg}}$  to have correctly decaying tunneling tails which are according to Eq. (27) relevant for the determination of the tunneling rates. While typically tunneling from the regular island occurs to regions within the chaotic sea close to the border of the regular island, there exist other cases, where it occurs to regions deeper inside the chaotic sea, as studied in Ref. [16]. Here  $H_{\text{reg}}$  has to be constructed such that its eigenstates have the correct tunneling tails up to this region.

For quantum maps we determine the fictitious integrable system in the following way: We employ classical methods, see below, to obtain a one-dimensional time-independent Hamiltonian  $H_{\text{reg}}(q, p)$  which is integrable by definition and resembles the classically regular motion corresponding to the mixed system. After its quantization we obtain the regular quantum map  $U_{\text{reg}} = e^{-iH_{\text{reg}}/h_{\text{eff}}}$  which has the same eigenfunctions  $|\psi_{\text{reg}}^m\rangle$  as  $H_{\text{reg}}$ . For the numerical evaluation of Eq. (27) we use  $P_{\text{ch}} = \mathbb{1} - P_{\text{reg}} = \mathbb{1} - \sum |\psi_{\text{reg}}^m\rangle\langle\psi_{\text{reg}}^m|$ , according to Eqs. (23) and (24), where the sum extends over  $m = 0, 1, \dots, N_{\text{reg}} - 1$ .

Two examples for the explicit construction of  $H_{\text{reg}}$  will be mentioned below. Note, that also other methods, e.g. based on the normal-form analysis [39, 40] or on the Campbell-Baker-Hausdorff formula [41] can be employed in order to find  $H_{\text{reg}}$ . For the example systems considered in this manuscript, however, they show less good agreement.

One possible choice for the determination of the fictitious integrable system for quantum maps is the Lie-transformation method [42]. It determines a classical Hamilton function as a series,

$$H_{\text{reg}}^K(q, p) = \sum_{l=1}^K h_l(q, p), \quad (29)$$

see Ref. [21] and Fig. 6(a) for an example. Typically, the order of the expansion  $K$  can be increased up to 20 within reasonable numerical effort. The Lie-transformation method provides a regular approximation  $H_{\text{reg}}$  which interpolates the dynamics inside the regular region and gives a smooth continuation into the chaotic sea. At some order  $K$  the series should diverge due to the nonlinear resonances inside the regular island. For strongly perturbed systems, such as the standard map at  $\kappa > 2.5$ , the Lie-transformation method may not be able to reproduce the regular dynamics of  $U$ , see Fig. 6(b). Here we use a method [17] based on the frequency map analysis [43].

An important question is whether the direct tunneling rates obtained using Eq. (27) depend on the actual choice of  $H_{\text{reg}}$  and how these results converge depending on the order  $K$  of its perturbation series. Ideally one would like to use classical measures, which describe the deviations of the regular system  $H_{\text{reg}}$  from the originally mixed one, to

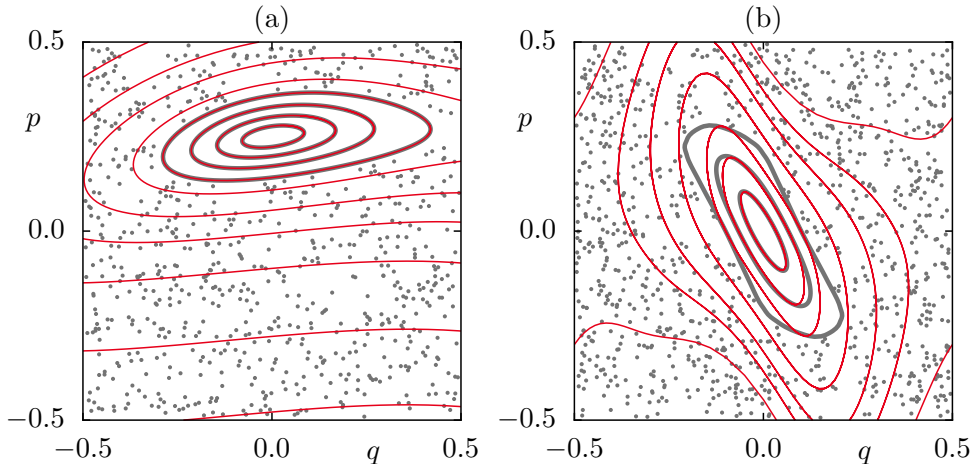


Figure 6: Application of the Lie transformation method: (a) Orbits (gray) of the map  $\mathcal{D}_d$  and of the corresponding integrable system (thin lines) of order  $K = 15$ . Here  $H_{\text{reg}}$  accurately resembles the regular dynamics of  $U$ . (b) Orbits of the standard map for  $\kappa = 2.9$  (gray) and of the corresponding integrable system (thin lines) of order  $K = 7$ . Here  $H_{\text{reg}}$  does not accurately resemble the regular dynamics of  $H$ .

predict the error of Eq. (27) for the tunneling rates. However, these classical measures can only account for the deviations within the regular region but not for the quality of the continuation of  $H_{\text{reg}}$  beyond the regular island of  $U$ . Currently, the quality of an integrable system can be estimated a posteriori by comparison of the predicted tunneling rates with numerical data. It remains an open question how to obtain a direct connection between the error on the classical side and the one for the tunneling rates.

### 3.3 Approximate fictitious integrable system

For an analytical evaluation of the result, Eq. (27), of the direct regular-to-chaotic tunneling rates we approximate the fictitious integrable system  $U_{\text{reg}}$  by a kicked system,  $\tilde{U}_{\text{reg}} = U_{\tilde{V}}U_T$  or  $\tilde{U}_{\text{reg}} = U_VU_{\tilde{T}}$  with

$$U_{\tilde{V}} = e^{-i\tilde{V}(q)/\hbar_{\text{eff}}}, \quad (30)$$

$$U_{\tilde{T}} = e^{-i\tilde{T}(p)/\hbar_{\text{eff}}}. \quad (31)$$

Here the functions  $\tilde{V}(q)$  and  $\tilde{T}(p)$  are a low order Taylor expansion of  $V(q)$  and  $T(p)$ , respectively, around the center of the regular island. Note, that the classical dynamics corresponding to  $\tilde{U}_{\text{reg}}$  is typically not completely regular. Still the following derivation is applicable if  $\tilde{U}_{\text{reg}}$  has the following properties: (i) Within the regular island it has an almost identical classical dynamics as  $U$ , including nonlinear resonances and small embedded chaotic regions. (ii) It shows mainly regular dynamics for a sufficiently wide region beyond the border of the regular island of  $U$ .

Now we consider the specific case  $\tilde{U}_{\text{reg}} = U_{\tilde{V}}U_T$  and assume that both properties (i) and (ii) are fulfilled. As the dynamics of  $U$  and  $\tilde{U}_{\text{reg}}$  are almost identical within the regular

island of  $U$ , the approximate result, Eq. (28), can be applied with  $U_{\text{reg}}$  replaced by  $\tilde{U}_{\text{reg}}$ , giving

$$\gamma_m \approx \|(U - U_{\tilde{V}}U_T)|\psi_{\text{reg}}^m\rangle\|^2 \quad (32)$$

$$= \|(UU_T^\dagger U_{\tilde{V}}^\dagger - \mathbf{1})U_{\tilde{V}}U_T|\psi_{\text{reg}}^m\rangle\|^2. \quad (33)$$

We now use that  $|\psi_{\text{reg}}^m\rangle$ , which is an eigenstate of the exact  $U_{\text{reg}}$  and  $H_{\text{reg}}$ , is an approximate eigenstate of  $U_{\tilde{V}}U_T$ , leading to  $U_{\tilde{V}}U_T|\psi_{\text{reg}}^m\rangle \approx e^{i\varphi_{\text{reg}}^m}|\psi_{\text{reg}}^m\rangle$ . With this we obtain

$$\gamma_m \approx \|(U_V U_{\tilde{V}}^\dagger - \mathbf{1})|\psi_{\text{reg}}^m\rangle\|^2. \quad (34)$$

In position representation this reads

$$\gamma_m \approx 2 \sum_{k=0}^{N-1} |\psi_{\text{reg}}^m(q_k)|^2 \left[ 1 - \cos\left(\frac{\Delta V(q_k)}{\hbar_{\text{eff}}}\right) \right], \quad (35)$$

where  $\Delta V(q) := V(q) - \tilde{V}(q)$  and  $q_k = k/N - 1/2$ . In the semiclassical limit the sum in Eq. (35) can be replaced by an integral

$$\gamma_m \approx 2 \int_{-1/2}^{1/2} dq |\psi_{\text{reg}}^m(q)|^2 \left[ 1 - \cos\left(\frac{\Delta V(q)}{\hbar_{\text{eff}}}\right) \right], \quad (36)$$

where we integrate over the whole position space  $q \in [-1/2, 1/2]$ . Note, that for the complementary situation, where  $U_{\text{reg}} \approx U_V U_{\tilde{T}}$  is used in Eq. (28), a similar result can be obtained in momentum representation

$$\gamma_m \approx 2 \int_{-1/2}^{1/2} dp |\psi_{\text{reg}}^m(p)|^2 \left[ 1 - \cos\left(\frac{\Delta T(p)}{\hbar_{\text{eff}}}\right) \right], \quad (37)$$

with  $\Delta T(p) := T(p) - \tilde{T}(p)$ .

We now use a WKB expression for the regular states  $|\psi_{\text{reg}}^m\rangle$ . For simplicity we restrict to the case  $H_{\text{reg}} = p^2/2 + W(q)$  leading to

$$\psi_{\text{reg}}^m(q) \approx \sqrt{\frac{\omega}{2\pi|p(q)|}} \exp\left(-\frac{1}{\hbar_{\text{eff}}} \int_{q_m^r}^q |p(q')| dq'\right), \quad (38)$$

which is valid for  $q > q_m^r$ . Here  $q_m^r$  is the right classical turning point of the  $m$ th quantizing torus,  $\omega$  is the oscillation frequency, and  $p(q) = \sqrt{2(E_{\text{reg}}^m - W(q))}$ . The eigenstates  $\psi_{\text{reg}}^m(q)$  decay exponentially beyond the classical turning point  $q_m^r$ . The difference of the potential energies  $\Delta V(q) = V(q) - \tilde{V}(q)$  approximately vanishes within the regular region and increases beyond its border to the chaotic sea. Hence, the most important contribution in

Eq. (36) arises near the left or the right border,  $q_b^l$  or  $q_b^r$ , of the regular island. For  $q > q_b^r$  we rewrite the regular states

$$\psi_{\text{reg}}^m(q) \approx \psi_{\text{reg}}^m(q_b^r) \exp\left(-\frac{1}{\hbar_{\text{eff}}} \int_{q_b^r}^q |p(q')| dq'\right) \sqrt{\frac{p(q_b^r)}{p(q)}} \quad (39)$$

$$\approx \psi_{\text{reg}}^m(q_b^r) \exp\left(-\frac{1}{\hbar_{\text{eff}}}(q - q_b^r)|p(q_b^r)|\right), \quad (40)$$

where in the last step we use  $p(q) \approx p(q_b^r)$  in the vicinity of the border.

In order to use Eq. (36) we split the integration interval in two parts, such that  $\gamma_m = \gamma_m^l + \gamma_m^r$ , corresponding to the contributions from the left and the right. We now approximate

$$\Delta V(q) \approx \begin{cases} 0 & , q_b^r \leq q \leq q_b^r \\ c_b(q - q_b^r) & , q > q_b^r \end{cases} \quad (41)$$

with some constant  $c_b$  and find

$$\gamma_m^r \approx 2\hbar_{\text{eff}} |\psi_{\text{reg}}^m(q_b^r)|^2 \int_0^{x_{\text{max}}} e^{-2x|p(q_b^r)|} [1 - \cos(c_b x)] dx \quad (42)$$

$$\approx \frac{I\hbar_{\text{eff}}}{\pi} |\psi_{\text{reg}}^m(q_b^r)|^2, \quad (43)$$

where  $x = (q - q_b^r)/\hbar_{\text{eff}}$  and  $x_{\text{max}} = (1/2 - q_b^r)/\hbar_{\text{eff}}$ . In the semiclassical limit  $x_{\text{max}} \rightarrow \infty$  and for fixed quantum number  $m$  the integral in Eq. (42),

$$I = \int_0^{x_{\text{max}}} e^{-2x|p(q_b^r)|} [1 - \cos(c_b x)] dx, \quad (44)$$

becomes an  $\hbar_{\text{eff}}$ -independent constant. The tunneling rate  $\gamma_m^r$  is proportional to the square of the modulus of the regular wave function at the right border  $q_b^r$  of the regular island. With Eq. (38) we obtain

$$\gamma_m^r \approx \frac{I\omega\hbar_{\text{eff}}}{2\pi^2|p(q_b^r)|} \exp\left(-\frac{2}{\hbar_{\text{eff}}} \int_{q_m^r}^{q_b^r} |p(q')| dq'\right). \quad (45)$$

A similar equation holds for  $\gamma_m^l$ .

As an example for the explicit evaluation of Eq. (45) we now consider the harmonic oscillator  $H_{\text{reg}}(p, q) = p^2/2 + \omega^2 q^2/2$ , where  $\omega$  denotes the oscillation frequency and gives the ratio of the two half axes of the elliptic invariant tori. Its classical turning points  $q_m^{r,l} = \pm\sqrt{2E_m}/\omega$ , the eigenenergies  $E_m = \hbar_{\text{eff}}\omega(m + 1/2)$ , and the momentum  $p(q) = \sqrt{2E_m - q^2\omega^2}$  are explicitly given. Using these expressions in Eq. (45) and  $\gamma_m = 2\gamma_m^r$  we obtain

$$\gamma_m = c \frac{\hbar_{\text{eff}}}{\beta_m} \exp\left(-\frac{2A}{\hbar_{\text{eff}}} \left[\beta_m - \alpha_m \ln\left(\frac{1 + \beta_m}{\sqrt{\alpha_m}}\right)\right]\right) \quad (46)$$

as the semiclassical prediction for the tunneling rate of the  $m$ th regular state, where  $\alpha_m = (m + 1/2)(A/h_{\text{eff}})^{-1}$ ,  $\beta_m = \sqrt{1 - \alpha_m}$ , and  $A$  is the area of the regular island. The exponent in Eq. (46) was also derived in Ref. [44]. The prefactor

$$c = \frac{I}{\pi^2} \sqrt{\frac{\pi\omega}{A}} \quad (47)$$

can be estimated semiclassically by solving the integral, Eq. (44), for  $x_{\text{max}} \rightarrow \infty$ . For a fixed classical torus of energy  $E$  one obtains

$$I \approx \frac{1}{2|p(q_b^r)|} - \frac{2|p(q_b^r)|}{4|p(q_b^r)|^2 + c_b^2}. \quad (48)$$

With this prefactor the prediction Eq. (46) gives excellent agreement with numerically determined data over 10 orders of magnitude in  $\gamma$ , see Fig. 7. For a fixed quantum number  $m$  the energy  $E_m$  goes to zero in the semiclassical limit such that one can approximate  $|p(q_b^r)| \approx \omega q_b^r$  in Eq. (48) which does not depend on  $h_{\text{eff}}$ .

Let us make the following remarks concerning Eq. (46): The only information about this non-generic island with constant rotation number is  $A/h_{\text{eff}}$  as in Ref. [15]. In contrast to Eq. (27) it does not require further quantum information such as the quantum map  $U$ . While the term in square brackets semiclassically approaches one, it is relevant for large  $h_{\text{eff}}$ . In contrast to Eq. (36), where the chaotic properties are contained in the difference  $V(q) - \tilde{V}(q)$ , they now appear in the prefactor  $c$  via the linear approximation of this difference.

In the semiclassical limit the tunneling rates predicted by Eq. (46) decrease exponentially. For  $h_{\text{eff}} \rightarrow 0$  the values  $\alpha_m$  go to zero and  $\beta_m$  to one, such that  $\gamma \sim e^{-2A/h_{\text{eff}}}$  remains which reproduces the qualitative prediction obtained in Ref. [14]. We find that the non-universal constant in the exponent is 2 which is comparable to the prefactor  $3 - \ln 4 \approx 1.61$  derived in Refs. [15, 45]. However, our result shows more accurate agreement to numerical data and does not require an additional fitting parameter, as will be shown in Sec. 4.

## 4 Applications

We study the direct regular-to-chaotic tunneling process in the systems introduced in Sec. 2 starting with the simplest example  $\mathcal{D}_{\text{ho}}$  with a harmonic oscillator-like regular island. As further systems, we consider the map  $\mathcal{D}_{\text{d}}$  with a deformed regular region, the map  $\mathcal{D}_{\text{rs}}$  with a regular stripe, and finally the standard map which shows a generic mixed phase space.

The map  $\mathcal{D}_{\text{ho}}$  has a particularly simple phase space structure with a harmonic oscillator-like regular island with elliptic invariant tori and constant rotation number, see the insets in Fig. 4. Numerically, we determine tunneling rates by using absorbing boundary conditions at  $|q| \geq 1/2$ . Analytically, for the approach derived in Sec. 3, Eq. (27), we use the Hamiltonian of a harmonic oscillator as the fictitious integrable system  $U_{\text{reg}}$ . It is squeezed and tilted according to the linearized dynamics in the vicinity of the stable fixed point located at the center of the regular island.

Figure 4 shows the prediction of Eq. (27) compared to numerical data. We find excellent agreement over more than 10 orders of magnitude in  $\gamma$ . In the regime of large

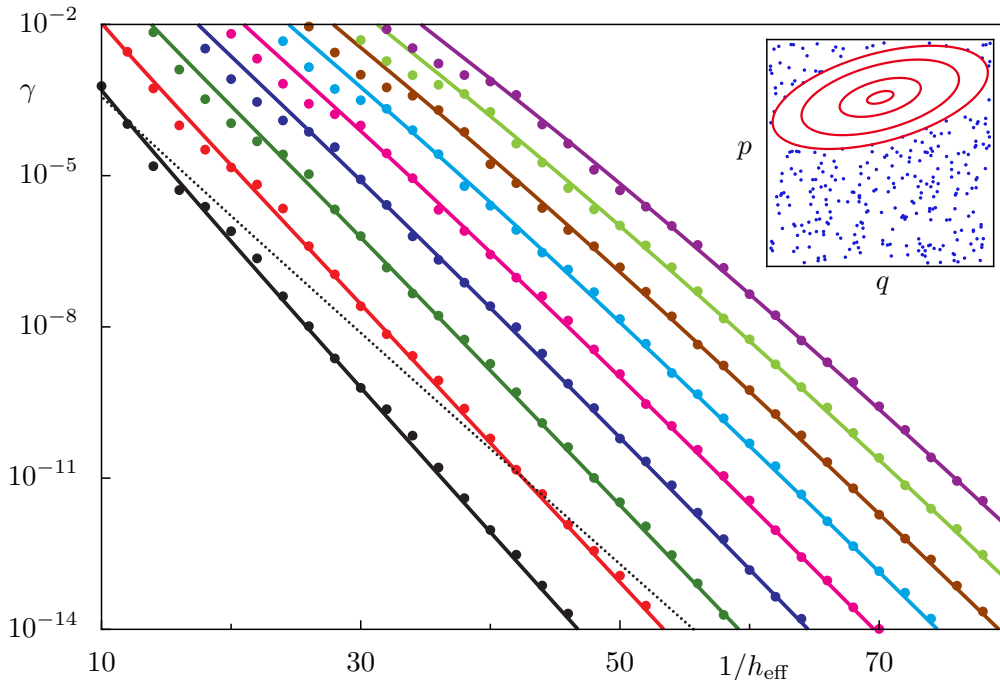


Figure 7: Numerical data (dots) for  $m \leq 8$  for the map  $\mathcal{D}_{\text{ho}}$  with a harmonic oscillator-like island. Comparison with Eq. (46) (solid lines). The prediction of Refs. [15, 45], Eq. (49), for  $m = 0$  with a fitted prefactor is shown (dotted line).

tunneling rates  $\gamma$  small deviations occur which can be attributed to the influence of the chaotic sea on the regular states: These states are located on quantizing tori close to the border of the regular island and are affected by the regular-to-chaotic transition region. However, the deviations in this regime are smaller than a factor of two.

In Fig. 7 we compare the results of the semiclassical prediction, Eq. (46), to the numerical data. Due to the approximations performed in the derivation of this formula stronger deviations are visible in the regime of large tunneling rates while the agreement in the semiclassical regime is still excellent.

In Refs. [15, 45] a prediction was derived for the tunneling rate of the regular ground state,

$$\gamma_0 = c \frac{\Gamma(\alpha, 4\alpha)}{\Gamma(\alpha, 0)}, \quad (49)$$

where  $\Gamma$  is the incomplete gamma function,  $\alpha = A/h_{\text{eff}}$ , and  $c$  is a constant. Eq. (49) can be approximated semiclassically (see Ref. [23]), leading to

$$\gamma_0 \propto e^{-\frac{A}{h_{\text{eff}}}(3-\ln 4)}. \quad (50)$$

Figure 7 shows the comparison of Eq. (49) (dotted line) to the numerical data for the map  $\mathcal{D}_{\text{ho}}$ . Especially in the semiclassical limit deviations are visible. The factor 2 which appears in the exponent of Eq. (46) is more accurate than the factor  $3 - \ln 4$  in Eq. (50).

In typical systems the rotation number of regular tori changes from the center of the regular region to its border which typically has a non-elliptic shape. Such a situation

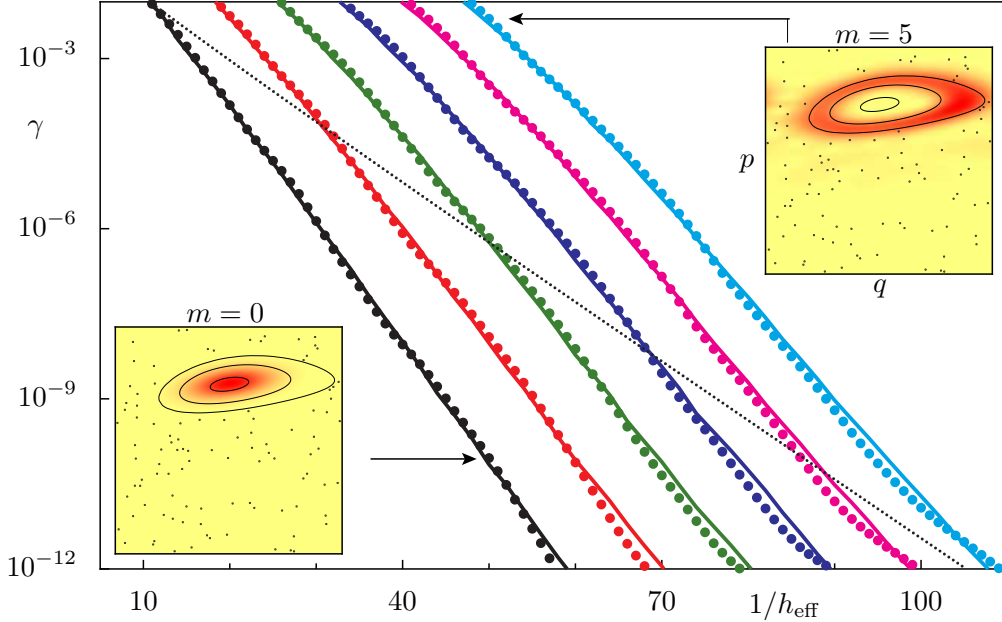


Figure 8: Dynamical tunneling rates from a regular island to the chaotic sea for the map  $\mathcal{D}_d$ : Numerical results (dots) and prediction following from Eq. (27) (lines) vs  $1/\hbar_{\text{eff}}$  for quantum numbers  $m \leq 5$ . The insets show Husimi representations of the regular states  $m = 0$  and  $m = 5$  at  $1/\hbar_{\text{eff}} = 50$ . The prediction of Refs. [15, 45], Eq. (49), for  $m = 0$  with a fitted prefactor is shown (dotted line).

can be achieved using the map  $\mathcal{D}_d$ . Here nonlinear resonances are small such that their influence on the tunneling process is expected only at large  $1/\hbar_{\text{eff}}$ , see the inset in Fig. 8 for its phase space.

We determine the fictitious integrable system  $H_{\text{reg}}$  by means of the Lie-transformation method described in Sec. 3.2. It is then quantized and its eigenfunctions are determined numerically. Fig. 8 shows a comparison of numerically determined tunneling rates (dots) to the prediction of Eq. (27) (solid lines) yielding excellent agreement for tunneling rates  $\gamma \gtrsim 10^{-11}$ . For smaller values of  $\gamma$  deviations occur due to resonance-assisted tunneling which is caused by a small 10:1 resonance chain. Similar to the case of the harmonic oscillator-like island the fictitious integrable system  $U_{\text{reg}}$  can be approximated by a kicked system  $U_{\text{reg}} \approx U_{\tilde{V}}U_{\text{T}}$  using  $\tilde{V}(q) = -rq^2/2 + Rq^3/3$ . Hence, Eqs. (35) and (36) can be evaluated giving similarly good agreement (not shown). The prediction of Eq. (49) [15, 45] (dotted line) shows large deviations to the numerical data.

We now consider the kicked system  $\mathcal{D}_{\text{rs}}$ , for which the regular region consists of a stripe in phase space, see the inset in Fig. 9. In Ref. [32] this map is used to study the evolution of a wave packet initially started in the regular region by means of complex paths. Also for this system one can predict tunneling rates by means of Eq. (27). The fictitious integrable system  $U_{\text{reg}}$  is determined by continuing the dynamics within  $|q| < q_d/(8\pi)$  to the whole

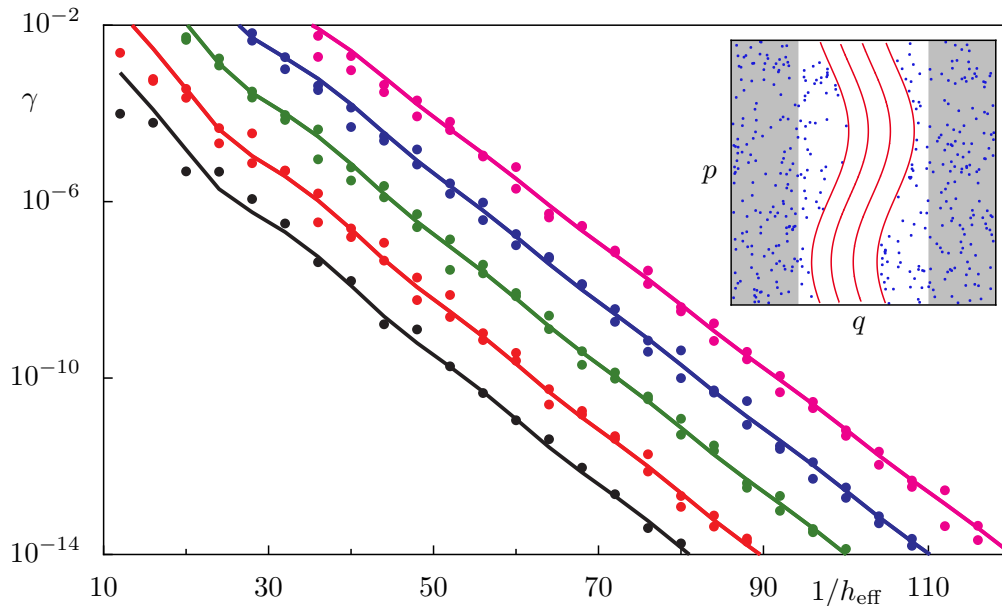


Figure 9: Dynamical tunneling rates from a regular stripe to the chaotic sea for the map  $\mathcal{D}_{rs}$ : We compare numerical results (dots) and the prediction following from Eq. (27) (lines) vs  $1/h_{\text{eff}}$  for the quantum numbers  $|m| \leq 4$ . The inset shows the phase space of the system. The numerical data is obtained using an absorbing region at  $|q| \geq 1/4$  (gray-shaded area of the inset).

phase space. It is given as a kicked system, Eq. (2), defined by the functions

$$\tilde{V}'(q) = -\frac{1}{2\pi} \left( \omega + \frac{d_1}{2} - \frac{d_2}{2} \right), \quad (51)$$

$$T'(p) = -\frac{\kappa}{8\pi} \sin(2\pi p). \quad (52)$$

For sufficiently large smoothing parameter  $b$ , see Eq. (10), the dynamics of the mixed map inside the regular region is equivalent to that of the regular map. Thus Eq. (27) can be applied and we compare its results to numerically determined data. Absorbing boundary conditions at  $|q| \geq 1/2$  lead to strong fluctuations of the numerically determined tunneling rates as a function of  $h_{\text{eff}}$ , presumably due to dynamical localization. Choosing  $|q| \geq 1/4$  for the opening, which is closer to the regular stripe, we find smoothly decaying tunneling rates, see Fig. 9. The comparison with the theoretical prediction shows quite good agreement. Note, that due to the symmetry of the map there are always two regular states with comparable tunneling rates except for the ground state  $m = 0$ . These two states are located symmetrically around the center of the regular stripe. While the theoretical prediction, Eq. (27), is identical for both of these states, the numerical results differ slightly due to the different chaotic dynamics in the vicinity of the left and right border of the regular region.

The paradigmatic model of an area preserving map is the standard map, see Sec. 2.1. For  $\kappa$  between 2.5 and 3.0 one has a large generic regular island with a relatively small hierarchical region surrounded by a 4:1 resonance chain, see the inset in Fig. 10. Absorbing

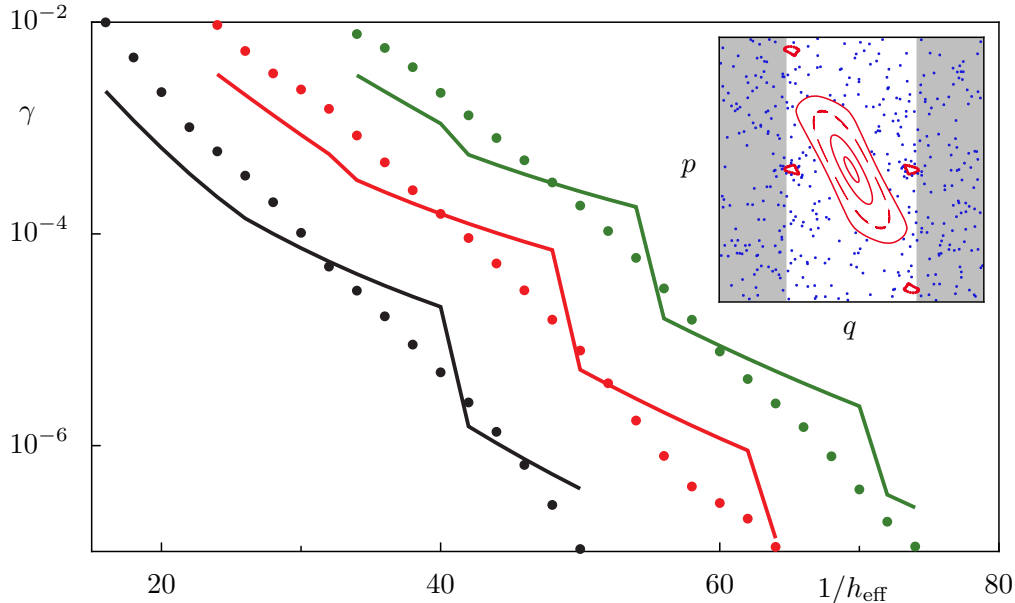


Figure 10: Tunneling rates for the standard map ( $\kappa = 2.9$ ) for  $m \leq 2$ . Prediction of Eq. (27) (lines) and numerical results (dots), obtained using an absorbing region at  $|q| \geq 1/4$  (gray-shaded area of the inset).

boundary conditions at  $|q| \geq 1/2$  lead to strong fluctuations of the numerically determined tunneling rates as a function of  $h_{\text{eff}}$ , presumably caused by partial barriers. Choosing absorbing boundary conditions at  $|q| \geq 1/4$ , which is closer to the island, we find smoothly decaying tunneling rates (dots in Fig. 10). Evaluating Eq. (27) for  $\kappa = 2.9$  gives good agreement with these numerical data, see Fig. 10 (solid lines). Here we determine  $H_{\text{reg}}$  using a method based on the frequency map analysis, as the Lie transformation is not able to reproduce the dynamics within the regular island of  $U$ , see Sec. 3.2. With increasing order of the expansion series of  $H_{\text{reg}}$  the tunneling rates following from Eq. (27) diverge. Hence, for the predictions in Fig. 10 we choose terms up to second order only. Note, that at such small order the accuracy of  $H_{\text{reg}}$  within the regular region of  $U$  is inferior compared to the examples discussed before. Hence, in Eq. (27) the state  $U|\psi_{\text{reg}}^m\rangle$  has small contributions of all purely regular states  $|\psi_{\text{reg}}^n\rangle$  in the regular island. These contributions are removed by the application of the projector  $P_{\text{ch}}$ . However, this projector depends on the number of regular states  $N_{\text{reg}}$ , which grows with  $1/h_{\text{eff}}$ . If  $N_{\text{reg}}$  increases by one,  $P_{\text{reg}}$  projects onto a larger region in phase space. This explains the steps of the theoretical prediction, Eq. (27), visible in Fig. 10.

## 5 Summary

Dynamical tunneling plays an important role in many areas of physics. Therefore a detailed understanding and quantitative description is of great interest. In this text we have given an overview on determining direct regular-to-chaotic tunneling rates using the fictitious integrable system approach. The direct regular-to-chaotic tunneling mechanism

is valid in the regime where Planck's constant is large compared to additional structures in the regular island, such as nonlinear resonances. To include the effect of such resonances, resonance-assisted tunneling [20, 22] has to be considered in addition with the direct regular-to-chaotic tunneling contribution. Recently, the two mechanisms have been studied in a combined theory [24], giving a full quantitative description of tunneling from a regular island, including resonances, into the chaotic region.

The approach to determine direct regular-to-chaotic tunneling rates can also be generalized to the case of billiard systems. It can be applied if the fictitious integrable system  $H_{\text{reg}}$  is known, as e.g. for the annular or the mushroom billiard. In addition to  $H_{\text{reg}}$  a description for the chaotic states of the mixed system  $H$  is needed, for which we employ random wave models [5] which account for the relevant boundary conditions of the billiard. For the mushroom billiard the fictitious integrable system is easily found as the semi-circle billiard and with this an analytical expression for the tunneling rates was derived in Ref. [18]. This result has been compared to experimental data obtained from microwave spectra of a mushroom billiard with adjustable stem height and good agreement was found. It was also shown that tunneling rates manifest themselves in exponentially diverging localization lengths of nanowires with one-sided surface roughness in a perpendicular magnetic field [46, 47].

The fictitious integrable system approach has been extended to open optical microcavities in Ref. [19]. In particular the annular microcavity was studied, which allows for unidirectional emission of light and shows modes of high quality factors simultaneously. This is desirable for most applications. In contrast to closed billiards the leakiness of the cavity has to be considered, which leads to the contribution  $Q_{\text{dir}}$  to the quality factor caused by the direct coupling of the regular mode to the continuum. Additionally, the contribution caused by dynamical tunneling  $Q_{\text{dyn}}$  is relevant, where  $1/Q = 1/Q_{\text{dir}} + 1/Q_{\text{dyn}}$ .  $Q_{\text{dyn}}$  is directly related to the dynamical tunneling rates given by the theory using a fictitious integrable system. The prediction for the quality factors  $Q$  has been compared to numerical data. Excellent agreement is found if no further phase-space structures exist in the chaotic sea. If additional structures appear, the numerical data show oscillations, which cannot be explained by the present theory.

Future challenges include a completely semiclassical prediction of direct regular-to-chaotic tunneling rates in generic systems, the understanding of implications of additional phase space structures, and the extension to higher dimensional systems.

## Acknowledgments

We are grateful to S. Creagh, S. Fishman, M. Hentschel, R. Höhmann, A. Köhler, U. Kuhl, A. Mouchet, M. Robnik, P. Schlagheck, A. Shudo, H.-J. Stöckmann, S. Tomsovic, G. Vidmar, and J. Wiersig for stimulating discussions. We further acknowledge financial support through the DFG Forschergruppe 760 "Scattering systems with complex dynamics".

## References

- [1] A. Bäcker, R. Ketzmerick, and S. Löck: *Direct Regular-to-Chaotic Tunneling Rates Using the Fictitious Integrable System Approach*, in *Dynamical Tunneling - Theory*

- and Experiment*, edited by S. Keshavamurthy and P. Schlagheck, pp. 119 - 137, Taylor and Francis CRC (2011).
- [2] L. D. Landau and E. M. Lifschitz: *Lehrbuch der theoretischen Physik, Band 3: Quantenmechanik*, Akademie Verlag, Berlin (1979).
  - [3] E. Gildener and A. Patrascioiu: *Pseudoparticle contributions to the energy spectrum of a one-dimensional system*, Phys. Rev. D **16**, 423–430 (1977).
  - [4] I. C. Percival: *Regular and irregular spectra*, J. Phys. B **6**, L229–L232 (1973).
  - [5] M. V. Berry: *Regular and irregular semiclassical wavefunctions*, J. Phys. A **10**, 2083–2091 (1977).
  - [6] A. Voros: in *Stochastic Behavior in Classical and Quantum Hamiltonian Systems*, Springer Verlag, Berlin (1979).
  - [7] M. J. Davis and E. J. Heller: *Quantum dynamical tunneling in bound states*, J. Chem. Phys. **75**, 246–254 (1981).
  - [8] W. A. Lin and L. E. Ballentine: *Quantum tunneling and chaos in a driven anharmonic oscillator*, Phys. Rev. Lett. **65**, 2927–2930 (1990).
  - [9] O. Bohigas, S. Tomsovic, and D. Ullmo: *Manifestations of classical phase space structures in quantum mechanics*, Phys. Rep. **223**, 43–133 (1993).
  - [10] S. Tomsovic and D. Ullmo: *Chaos-assisted tunneling*, Phys. Rev. E **50**, 145–162 (1994).
  - [11] C. Dembowski, H.-D. Gräf, A. Heine, R. Hofferbert, H. Rehfeld, and A. Richter: *First Experimental Evidence for Chaos-Assisted Tunneling in a Microwave Annular Billiard*, Phys. Rev. Lett. **84**, 867–870 (2000).
  - [12] D. A. Steck, W. H. Oskay, and M. G. Raizen: *Observation of chaos-assisted tunneling between islands of stability*, Science **293**, 274–278 (2001).
  - [13] W. K. Hensinger, H. Häffner, A. Browaeys, N. R. Heckenberg, K. Helmerson, C. McKenzie, G. J. Milburn, W. D. Phillips, S. L. Rolston, H. Rubinsztein-Dunlop, and B. Upcroft: *Dynamical tunnelling of ultracold atoms*, Nature **412**, 52–55 (2001).
  - [14] J. D. Hanson, E. Ott, and T. M. Antonsen: *Influence of finite wavelength on the quantum kicked rotator in the semiclassical regime*, Phys. Rev. A **29**, 819–825 (1984).
  - [15] V. A. Podolskiy and E. E. Narimanov: *Semiclassical Description of Chaos-Assisted Tunneling*, Phys. Rev. Lett. **91**, 263601 (2003).
  - [16] M. Sheinman, S. Fishman, I. Guarneri, and L. Rebuffini: *Decay of quantum accelerator modes*, Phys. Rev. A **73**, 052110 (2006).
  - [17] A. Bäcker, R. Ketzmerick, S. Löck, and L. Schilling: *Regular-to-chaotic tunneling rates using a fictitious integrable system*, Phys. Rev. Lett. **100**, 104101 (2008).

- [18] A. Bäcker, R. Ketzmerick, S. Löck, M. Robnik, G. Vidmar, R. Höhmann, U. Kuhl, and H.-J. Stöckmann: *Dynamical tunneling in mushroom billiards*, Phys. Rev. Lett. **100**, 174103 (2008).
- [19] A. Bäcker, R. Ketzmerick, S. Löck, J. Wiersig, and M. Hentschel: *Quality factors and dynamical tunneling in annular microcavities*, Phys. Rev. A **79**, 063804 (2009).
- [20] O. Brodier, P. Schlagheck, and D. Ullmo: *Resonance-assisted tunneling in near-integrable systems*, Phys. Rev. Lett. **87**, 064101 (2001).
- [21] O. Brodier, P. Schlagheck, and D. Ullmo: *Resonance-Assisted Tunneling*, Ann. of Phys. **300**, 88–136 (2002).
- [22] C. Eltschka and P. Schlagheck: *Resonance- and Chaos-Assisted Tunneling in Mixed Regular-Chaotic Systems*, Phys. Rev. Lett. **94**, 014101 (2005).
- [23] P. Schlagheck, C. Eltschka, and D. Ullmo: *Resonance- and Chaos-Assisted Tunneling*, in *Progress in Ultrafast Intense Laser Science I*, edited by K. Yamanouchi, S. L. Chin, P. Agostini, and G. Ferrante, Springer, Berlin (2006).
- [24] S. Löck, A. Bäcker, R. Ketzmerick, and P. Schlagheck: *Regular-to-Chaotic Tunneling Rates: From the Quantum to the Semiclassical Regime*, Phys. Rev. Lett. **104**, 114101 (2010).
- [25] M. V. Berry: *Regular and irregular motion*, Am. Inst. Phys. Conf. Proc. **46**, 16–120 (1978).
- [26] D. K. Arrowsmith and C. M. Place: *An introduction to dynamical systems*, Cambridge University Press, Cambridge (1990).
- [27] R. S. MacKay, J. D. Meiss, and I. C. Percival: *Transport in Hamiltonian systems*, Physica D **13**, 55–81 (1984).
- [28] H. Schanz, M.-F. Otto, R. Ketzmerick, and T. Dittrich: *Classical and Quantum Hamiltonian Ratchets*, Phys. Rev. Lett. **87**, 070601 (2001).
- [29] A. Bäcker, R. Ketzmerick, and A. G. Monastra: *Flooding of Chaotic Eigenstates into Regular Phase Space Islands*, Phys. Rev. Lett. **94**, 054102 (2005).
- [30] A. Shudo and K. S. Ikeda: *Complex Classical Trajectories and Chaotic Tunneling*, Phys. Rev. Lett. **74**, 682–685 (1995).
- [31] A. Shudo and K. S. Ikeda: *Chaotic tunneling: A remarkable manifestation of complex classical dynamics in non-integrable quantum phenomena*, Physica D **115**, 234–292 (1998).
- [32] A. Ishikawa, A. Tanaka, and A. Shudo: *Quantum suppression of chaotic tunneling*, J. Phys. A. **40**, F397–F405 (2007).
- [33] M. V. Berry, N. L. Balzas, M. Tabor, and A. Voros: *Quantum Maps*, Ann. of Phys. **122**, 26–63 (1979).

- [34] S.-J. Chang and K.-J. Shi: *Evolution and exact eigenstates of a resonant quantum system*, Phys. Rev. A **34**, 7–22 (1986).
- [35] H. Schomerus and J. Tworzydło: *Quantum-to-Classical Crossover of Quasibound States in Open Quantum Systems*, Phys. Rev. Lett. **93**, 154102 (2004).
- [36] M. Wilkinson: *Tunnelling between tori in phase space*, Physica D **21**, 341–354 (1986).
- [37] S. C. Creagh: *Tunneling in two dimensions*, in *Tunneling in Complex Systems*, World Scientific, Singapore (1998).
- [38] T. Onishi, A. Shudo, K. S. Ikeda, and K. Takahashi: *Tunneling mechanism due to chaos in a complex phase space*, Phys. Rev. E **64**, 025201 (2001).
- [39] F. G. Gustavson: *On constructing formal integrals of a Hamiltonian system near an equilibrium point*, The Astronomical Journal **71**, 670–686 (1966).
- [40] A. Bazzani, M. Giovannozzi, G. Servizi, E. Todesco, and G. Turchetti: *Resonant normal forms, interpolating Hamiltonians and stability of area preserving maps*, Physica D **64**, 66–97 (1993).
- [41] R. Scharf: *Quantum maps, adiabatic invariance and the semiclassical limit*, J. Phys. A **21**, 4133–4147 (1988).
- [42] A. J. Lichtenberg and M. A. Leiberman: *Regular and Stochastic Motion*, Springer, New York (1983).
- [43] J. Laskar, C. Froeschlé, and A. Celletti: *The means of chaos by the numerical analysis of the fundamental frequencies. Application to the standard mapping*, Physica D **56**, 253–269 (1992).
- [44] J. L. Deunff and A. Mouchet: *Instantons re-examined: Dynamical tunneling and resonant tunneling*, Phys. Rev. E **81**, 046205 (2010).
- [45] M. Sheinman: *Decay of Quantum Accelerator Modes*, Master Thesis, Technion, Haifa, Israel (2005).
- [46] J. Feist, A. Bäcker, R. Ketzmerick, S. Rotter, B. Huckestein, and J. Burgdörfer: *Nano-wires with surface disorder: Giant localization lengths and quantum-to-classical crossover*, Phys. Rev. Lett. **97**, 116804 (2006).
- [47] J. Feist, A. Bäcker, R. Ketzmerick, J. Burgdörfer, and S. Rotter: *Nanowires with surface disorder: Giant localization length and dynamical tunneling in the presence of directed chaos*, Phys. Rev. B **80**, 245322 (2009).